Bragg reflection waveguides with a matching layer

Amit Mizrahi and Levi Schächter
Electrical Engineering Department, Technion–IIT, Haifa 32000, ISRAEL
amitmiz@tx.technion.ac.il

Abstract: It is demonstrated that Bragg reflection waveguides, either planar or cylindrical, can be designed to support a symmetric mode with a specified core field distribution, by adjusting the first layer width. Analytic expressions are given for this *matching layer*, which matches between the electromagnetic field in the core, and a Bragg mirror optimally designed for the mode. This adjustment may change significantly the characteristics of the waveguide. At the particular wavelength for which the waveguide is designed, the electromagnetic field is identical to that of a partially dielectric loaded metallic or perfect magnetic waveguide, rather than a pure metallic waveguide. Either a planar or coaxial Bragg waveguide is shown to support a mode that has a TEM field distribution in the hollow region.

OCIS codes: (130.2790) Guided waves; (230.1480) Bragg reflectors; (230.7370) Optical design and fabrication.

References and links

1. P. Yeh and A. Yariv, "Bragg reflection waveguides," Opt. Commun. **19**, 427–430 (1976).
2. P. Yeh, A. Yariv, and E. Marom, "Theory of Bragg fiber," J. Opt. Soc. Am. **68**, 1196–1201 (1978).
3. Y. Fink, D. J. Ripin, S. Fan, C. Chen, J. D. Joannopoulos, and E. L. Thomas, "Guiding optical light in air using an all-dielectric structure," J. Lightwave Technol. **17**, 2039–2041 (1999).
4. B. Temelkuran, S. D. Hart, G. Benoit, J. D. Joannopoulos, and Y. Fink, "Wavelength-scalable hollow optical fibres with large Photonic bandgaps for CO_2 laser transmission," Nature **420**, 650–653 (2002).
5. S. G. Johnson, M. Ibanescu, M. Skorobogatiy, O. Weisberg, T. D. Engeness, M. Soljačić, S. A. Jacobs, J. D. Joannopoulos, and Y. Fink, "Low-loss asymptotically single-mode propagation in large-core Omniguide fibers," Opt. Express **9**, 748–779 (2001). http://www.opticsexpress.org/abstract.cfm?URI=OPEX-9-13-748.
6. M. Ibanescu, S. G. Johnson, M. Soljačić, J. D. Joannopoulos, Y. Fink, O. Weisberg, T. D. Engeness, S. A. Jacobs, and M. Skorobogatiy, "Analysis of mode structure in hollow dielectric waveguide fibers," Phys. Rev. E **67**, 046,608 (2003).
7. Y. Xu, R. K. Lee, and A. Yariv, "Asymptotic analysis of Bragg fibers," Opt. Lett. **25**, 1756–1758 (2000).
8. Y. Xu, G. X. Ouyang, R. K. Lee, and A. Yariv, "Asymptotic matrix theory of Bragg fibers," J. Lightwave Tech. **20**, 428–440 (2002).
9. Y. Xu and A. Yariv, "Asymptotic analysis of Silicon based Bragg fibers," Opt. Express **11**, 1039–1049 (2003). http://www.opticsexpress.org/abstract.cfm?URI=OPEX-11-9-1039.
10. G. Ouyang, Y. Xu, and A. Yariv, "Theoretical study on dispersion compensation in air-core Bragg fibers," Opt. Express **10**, 899–908 (2002). http://www.opticsexpress.org/abstract.cfm?URI=OPEX-10-17-899.
11. M. Ibanescu, Y. Fink, S. Fan, E. L. Thomas, and J. D. Joannopoulos, "An all-dielectric coaxial waveguide," Science **289**, 415–419 (2000).
12. Y. Xu, R. K. Lee, and A. Yariv, "Asymptotic analysis of dielectric coaxial fibers," Opt. Lett. **27**, 1019–1021 (2002).
13. G. Ouyang, Y. Xu, and A. Yariv, "Comparative study of air-core and coaxial Bragg fibers: single-mode transmission and dispersion characteristics," Opt. Express **9**, 733–747 (2001). http://www.opticsexpress.org/abstract.cfm?URI=OPEX-9-13-733.
14. T. D. Engeness, M. Ibanescu, S. G. Johnson, O. Weisberg, M. Skorobogatiy, S. Jacobs, and Y. Fink, "Dispersion tailoring and compensation by modal interactions in Omniguide fibers," Opt. Express **11**, 1175–1196 (2003). http://www.opticsexpress.org/abstract.cfm?URI=OPEX-11-10-1175.

#4356 - $15.00 US
Received 27 May 2004; revised 1 July 2004; accepted 1 July 2004

15. A. Mizrahi and L. Schächter, "Optical Bragg accelerators," Phys. Rev. E (to be published) (2004).
16. F. Benabid, J. C. Knight, and P. S. J. Russell, "Particle levitation and guidance in hollow-core photonic crystal fiber," Opt. Express **10**, 1195–1203 (2002). http://www.opticsexpress.org/abstract.cfm?URI=OPEX-10-21-1195.
17. G. Lenz, E. Baruch, and J. Salzman, "Polarization discrimination properties of Bragg-reflection waveguides," Opt. Lett. **15**, 1288–1290 (1990).
18. C. M. de Sterke, I. M. Bassett, and A. G. Street, "Differential losses in Bragg fibers," J. Appl. Phys. **76**, 680–688 (1994).
19. P. Yeh, "Electromagnetic propagation in birefringent layered media," J. Opt. Soc. Am. **65**, 742–756 (1979).

1. Introduction

Bragg reflection waveguides are one-dimensional photonic band-gap structures, designed to guide light in a low refractive index region surrounded by high refractive index alternating dielectric layers. Two possible configurations are depicted in Fig. 1, one is the planar Bragg reflection waveguide, and the other is the cylindrical, which is also known as the *Bragg Fiber*. The theory of Bragg reflection waveguides was developed by Yeh *et al*. [1, 2], and recently there has been a growing interest in using such hollow cylindrical structures as low-loss optical fibers in long distance communications. Fabrication of such fibers was demonstrated [3, 4]. The propa-

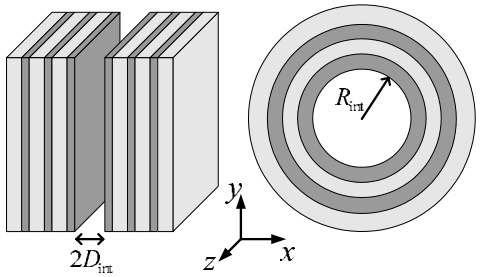

Fig. 1. Planar and cylindrical Bragg reflection waveguides.

gation characteristics were investigated and compared with those of metallic waveguides [5, 6]. In general, for large radii, there is a resemblance between the cylindrical and the planar structures, enabling asymptotic analysis methods [7, 8, 9]. For dispersion compensation purposes it was shown that high dispersion values can be achieved in small-core Bragg fibers [10]. A variation of the Bragg fiber is the dielectric coaxial fiber which has dielectric core and cladding, and a hollow region between them [11, 12, 13]. While most of the studies carried out on Bragg reflection waveguides dealt with configurations where all the dielectric layers are transverse quarter-wave thick, it was demonstrated that by creating a defect in the form of changing one or more of the layer widths, it is possible to influence the dispersion properties of the fiber [14].

In a recent study, the planar and cylindrical Bragg reflection waveguides with a vacuum core were suggested as future optical particle accelerators driven by high power lasers [15]. For a waveguide to serve as a particle accelerator, it is necessary that a TM mode with phase velocity that equals the speed of light ($v_{\text{ph}} = c$) is supported. As discussed in other studies, when all the layers are taken to be transverse quarter-wavelength thick, the supported mode resembles that of a metallic waveguide. Obviously, the phase velocity in this case is greater than c. In Ref. [15] it was shown that by changing the width of the layer adjacent to the vacuum core, a mode with $v_{\text{ph}} = c$ is supported. In the present study we generalize the concept of this *matching layer* to any given phase velocity (or field distribution) and to both TE and TM modes. Analytic expressions are given for the width of the matching layer as part of a design procedure that achieves two goals *simultaneously*: (1) the specified core field distribution at a given wavelength and a given core dimension is an eigen-mode of the structure (2) the transverse exponential decay in the

#4356 - $15.00 US
Received 27 May 2004; revised 1 July 2004; accepted 1 July 2004

Table 1. Hollow core symmetric modes. The transverse wavenumbers are $k_{x,r} = \sqrt{\omega^2/c^2 - k_z^2}$.

	General symmetric mode	Special case $v_{\rm ph} = c$
Planar TM	$E_z = E_0 \cos(k_x x) e^{-jk_z z}$ $E_x = j\frac{k_z}{k_x} E_0 \sin(k_x x) e^{-jk_z z}$ $H_y = j\frac{\omega}{c}\frac{1}{\eta_0 k_x} E_0 \sin(k_x x) e^{-jk_z z}$	$E_z = E_0 e^{-j\frac{\omega}{c}z}$ $E_x = j\frac{\omega}{c} x E_0 e^{-j\frac{\omega}{c}z}$ $H_y = \frac{j}{\eta_0}\frac{\omega}{c} x E_0 e^{-j\frac{\omega}{c}z}$
Planar TE	$H_z = H_0 \cos(k_x x) e^{-jk_z z}$ $H_x = j\frac{k_z}{k_x} H_0 \sin(k_x x) e^{-jk_z z}$ $E_y = -j\frac{\omega}{c}\frac{\eta_0}{k_x} H_0 \sin(k_x x) e^{-jk_z z}$	$H_z = H_0 e^{-j\frac{\omega}{c}z}$ $H_x = j\frac{\omega}{c} x H_0 e^{-j\frac{\omega}{c}z}$ $E_y = -j\eta_0\frac{\omega}{c} x H_0 e^{-j\frac{\omega}{c}z}$
Cylindrical TM	$E_z = E_0 J_0(k_r r) e^{-jk_z z}$ $E_r = j\frac{k_z}{k_r} E_0 J_1(k_r r) e^{-jk_z z}$ $H_\phi = j\frac{\omega}{c}\frac{1}{\eta_0 k_r} E_0 J_1(k_r r) e^{-jk_z z}$	$E_z = E_0 e^{-j\frac{\omega}{c}z}$ $E_r = \frac{j}{2}\frac{\omega}{c} r E_0 e^{-j\frac{\omega}{c}z}$ $H_\phi = \frac{j}{2\eta_0}\frac{\omega}{c} r E_0 e^{-j\frac{\omega}{c}z}$
Cylindrical TE	$H_z = H_0 J_0(k_r r) e^{-jk_z z}$ $H_r = j\frac{k_z}{k_r} H_0 J_1(k_r r) e^{-jk_z z}$ $E_\phi = -j\frac{\omega}{c}\frac{\eta_0}{k_r} H_0 J_1(k_r r) e^{-jk_z z}$	$H_z = H_0 e^{-j\frac{\omega}{c}z}$ $H_r = \frac{j}{2}\frac{\omega}{c} r H_0 e^{-j\frac{\omega}{c}z}$ $E_\phi = -\frac{j\eta_0}{2}\frac{\omega}{c} r H_0 e^{-j\frac{\omega}{c}z}$

Bragg mirror is the strongest possible. Hence, the first layer matches between the core mode and the Bragg mirror mode. The core dimension itself may be dictated by other considerations, such as the maximum field which is allowed to develop at the vacuum-dielectric interface to prevent breakdown, and interaction efficiency constraints [15].

The ability to design the waveguide to support specified field profiles in the core may be useful in applications other than particle accelerators, such as high power laser waveguides or dielectric particle levitation [16]. The basic modes of interest are the symmetric modes, TM and TE, the hollow core field distributions of which are summarized in Table 1. As a special case which receives relatively little attention in waveguide literature, the fields of $v_{\rm ph} = c$ are written explicitly. Demonstration of the principles presented here will be on waveguides made from dielectric materials with refractive indices 1.6 and 4.6, as was used in Refs. [5, 6, 3, 7]. Throughout this study we neglect the losses due to the finite cladding; a discussion of this loss effect may be found in Refs. [2, 17, 18, 5].

In Section 2 a general method for the design of a Bragg reflection waveguide, either planar or cylindrical is presented, in which the layer adjacent to the core is adjusted. Section 3 deals with the effect of the matching layer on the properties of the waveguide. Section 4 presents an extension of the previous formulation to planar odd modes, which enables the design of useful power profiles in the core. Section 5 discusses the possibility of guiding a mode which has a TEM field distribution within the hollow core, in both planar waveguides and coaxial dielectric waveguides.

2. Formulation

2.1. Matching layer in a planar waveguide

We first consider a *planar* Bragg reflection waveguide ($\partial/\partial y = 0$), with core half-width $D_{\rm int}$, as depicted in the left frame of Fig. 1. Let us assume that at some specific wavelength λ_0 with a corresponding angular frequency ω_0, this waveguide is required to support a symmetric TM mode with a specific phase velocity $v_{\rm ph} = \omega_0/k_z$, k_z being the longitudinal wavenumber. Equivalently, a specific field distribution in the hollow core may be required, determined by the transverse

#4356 - $15.00 US
Received 27 May 2004; revised 1 July 2004; accepted 1 July 2004

wavenumber $k_x = \sqrt{\omega^2/c^2 - k_z^2}$, as shown in Table 1. Expressing the phase velocity in terms of the transverse wavenumber in the core, we obtain $v_{\rm ph} = c/\sqrt{1-(k_x\lambda_0/2\pi)^2}$. The longitudinal electric field in the layer adjacent to the core, which has a dielectric coefficient ε_1, is given by $E_z = \left(A_1 e^{-jk_1 x} + B_1 e^{+jk_1 x}\right) e^{-jk_z z}$, where the transverse wavenumber is $k_1 = \sqrt{\omega^2/c^2\varepsilon_1 - k_z^2}$, and the transverse impedance is $Z_1 = k_1/(\omega\varepsilon_0\varepsilon_1)$. The required electromagnetic field in the vacuum core dictates by virtue of the boundary conditions on E_z and H_y at the interface between the core and the adjacent dielectric layer, the amplitudes in the first layer. Imposing the boundary conditions on E_z and H_y at $x = D_{\rm int}$, the amplitudes are found to be given by

$$A_1/E_0 = (B_1/E_0)^* = \frac{1}{2} e^{jk_1 D_{\rm int}} \cos(k_x D_{\rm int}) - j\frac{k_1}{2\varepsilon_1 k_x} e^{jk_1 D_{\rm int}} \sin(k_x D_{\rm int}); \tag{1}$$

the asterik denotes complex conjugate, and E_0 is defined in Table 1. It is now our purpose to ensure that the complete structure including the Bragg reflector indeed supports the required field at the given wavelength as an eigen-mode.

The Bragg reflector can be analyzed from the perspective of a pure periodic structure according to the Floquet theorem [1]. This analysis gives the eigen-values and the eigen-vectors of the periodic structure, and determines the band-gaps of the system, where the two eigen-values absolute values are different than unity, leading to a decay or growth in the waves amplitudes. The strongest exponential decay is found to be when each material of the two is chosen to be a quarter of wavelength thick. In case of a Bragg reflection waveguide it is a quarter of the transverse wavelength, meaning that this thickness of layer ν with dielectric coefficient ε_ν is given by

$$\Delta_\nu = \frac{\pi}{2\sqrt{\frac{\omega_0^2}{c^2}\varepsilon_\nu - k_z^2}}. \tag{2}$$

The eigen-values in this optimal decay case are given by the ratios of the two transverse impedances in the two materials. The corresponding eigen-vectors indicate that at every interface between two dielectrics, each one of the electromagnetic field components either peaks or vanishes, according to the type of transition, high to low, or low to high impedance. This condition was originally mentioned in Ref. [2], and is more recently emphasized in Ref. [15].

Going back to the Bragg reflection waveguide, since the amplitudes in the first dielectric layer are already known, the interface between the first and the second dielectric layers may be considered as an entrance to a periodic structure, to which the wave must enter in one of the eigen-vectors for the mode to be supported, or in other words, a perfect reflection must occur at the interface between the first and the second layers. Explicitly, this condition is given by

$$\begin{cases} E_z(x = D_{\rm int} + \Delta_1) = 0 & Z_1 > Z_2 \\ \dfrac{\partial E_z}{\partial x}(x = D_{\rm int} + \Delta_1) = 0 & Z_1 < Z_2\,, \end{cases} \tag{3}$$

where Δ_1 is the first layer width, and Z_1, Z_2 are the transverse impedances of the first and second layers respectively. Setting the first layer width according to the above condition will ensure that the required mode at the given wavelength will indeed be supported by the waveguide. The first layer may therefore be conceived as a *matching layer* between the vacuum region and the subsequent periodic structure, as it rotates the amplitude vector dictated by the vacuum mode, to overlap the eigen-vector of the periodic structure.

Given the amplitudes, as required by Eq. (1), it is now straightforward to determine the points

#4356 - $15.00 US
Received 27 May 2004; revised 1 July 2004; accepted 1 July 2004

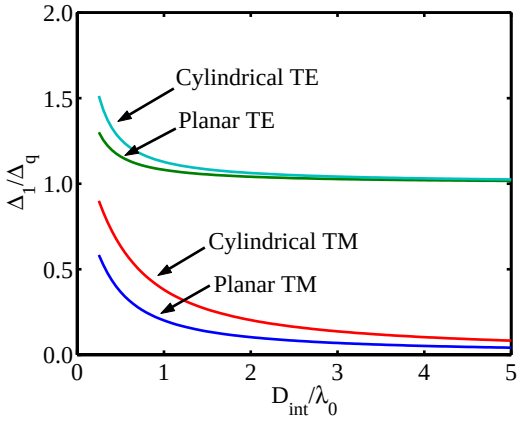

Fig. 2. First layer width for $v_{ph} = c$, normalized by $\Delta_q \triangleq \lambda_0/(4\sqrt{\varepsilon_1 - 1})$. The layer adjacent to the core has a refractive index of $n_1 = 1.6$ and the other material has $n_2 = 4.6$.

where E_z peaks or vanishes. The resulting expression for the first layer width reads

$$\Delta_1^{(\mathrm{TM})} = \begin{cases} \dfrac{1}{k_1} \arctan\left[\dfrac{\varepsilon_1 k_x}{k_1} \cot(k_x D_{\mathrm{int}})\right] & Z_1 > Z_2 \\ \dfrac{1}{k_1} \arctan\left[-\dfrac{k_1}{\varepsilon_1 k_x} \tan(k_x D_{\mathrm{int}})\right] & Z_1 < Z_2\,. \end{cases} \tag{4}$$

In the above expression, the smallest positive value of the arctan function is chosen. It should be noted that k_x may be purely imaginary, meaning that the transverse waves in the core are evanescent, and the expression still holds, as long as the transverse wavenumbers in the dielectric layers are real. A special case of this expression is when $k_x D_{\mathrm{int}} = \pi, \pi/2$, and then the matching layer is transverse quarter-wavelength thick similarly to the outer layers. For the special case where the phase velocity equals the speed of light ($k_z = \omega_0/c$), the expression for the first layer width simplifies to read

$$\Delta_1^{(\mathrm{TM})} = \begin{cases} \dfrac{1}{k_1} \arctan\left[\left(\dfrac{Z_1}{\eta_0} \dfrac{\omega_0}{c} D_{\mathrm{int}}\right)^{-1}\right] & Z_1 > Z_2 \\ \dfrac{1}{k_1} \arctan\left(-\dfrac{Z_1}{\eta_0} \dfrac{\omega_0}{c} D_{\mathrm{int}}\right) & Z_1 < Z_2\,. \end{cases} \tag{5}$$

Figure 2 illustrates at the bottom curve the planar TM first layer width as a function of the core half-width D_{int}, for the requirement that $v_{ph} = c$. The first layer was set to have a refractive index of $n_1 = \sqrt{\varepsilon_1} = 1.6$, and the other material was taken to be of refractive index $n_2 = \sqrt{\varepsilon_2} = 4.6$. The first layer width is normalized by $\Delta_q \triangleq \lambda_0/(4\sqrt{\varepsilon_1 - 1})$, which is the transverse quarter-wavelength width in the $v_{ph} = c$ case. The choice of placing the lower refractive index first entails that the first case of Eq. (5) is used in the calculation of the planar TM first layer width.

The same principles can easily be implemented for TE modes, planar and cylindrical. From the requirement that H_z either peaks or vanishes, the planar TE matching layer width is found to be

$$\Delta_1^{(\mathrm{TE})} = \begin{cases} \dfrac{1}{k_1} \arctan\left[\dfrac{k_x}{k_1} \cot(k_x D_{\mathrm{int}})\right] & Y_1 > Y_2 \\ \dfrac{1}{k_1} \arctan\left[-\dfrac{k_1}{k_x} \tan(k_x D_{\mathrm{int}})\right] & Y_1 < Y_2\,, \end{cases} \tag{6}$$

#4356 - $15.00 US
Received 27 May 2004; revised 1 July 2004; accepted 1 July 2004

where $Y_{1,2} = k_{1,2}/(\omega_0\mu_0)$ are the transverse admittances, and $k_{1,2}$ are the transverse wavenumbers in the first and second layers. The difference between the above expression and the TM expression is a ε_1 factor in the arctan argument. The second curve from the top of Fig. 2 illustrates the planar TE case. It is seen that the TM curve approaches zero, whereas the TE curve is above the $\Delta_1/\Delta_q = 1$ line and approaches unity for large core widths. This situation is reversed according to the given analytical expressions, should the material of the layer adjacent to the core is chosen to be of the higher refractive index of the two mentioned.

To summarize, the design procedure described here is as follows. According to the required k_z, a Bragg mirror is designed so that all layers are transverse quarter-wavelength thick. In order to match the mirror to the desired core field, the layer adjacent to the core is adjusted to the width given above by analytic expressions.

2.2. Matching layer in a cylindrical waveguide

Although the periodic structure approach utilized for the planar Bragg reflection waveguide is not suitable for the cylindrical case, some of the results still hold. As shown in Ref. [2], the condition given by Eq. (3) can be obtained for the cylindrical case in a process of minimization of the average energy density, when designing the structure from the inside out. Explicitly, at the interface between an inner layer ν to an outer layer $\nu+1$, the longitudinal electric field should satisfy the condition

$$\begin{cases} E_z = 0 & Z_\nu > Z_{\nu+1} \\ \dfrac{\partial E_z}{\partial r} = 0 & Z_\nu < Z_{\nu+1}\,. \end{cases} \tag{7}$$

Asymptotically, this condition is equivalent to the transverse quarter-wavelength widths, but once again it has an implication on the width of the layer adjacent to the core. Imposing the boundary conditions from the inside out around a desired field distribution in the core, and setting the interfaces between the dielectrics to fulfill the above condition, constitutes a design procedure. In practice, only the first layer may differ significantly from the transverse quarter-wavelength, and the outer layers will have a difference of a few percent at most. The approach of designing the structure from the inside out is more general than the one presented in the last section, and it holds for both the planar and the cylindrical case.

Following the same formulation as for the planar case, the longitudinal electric field in the first layer, assuming TM mode, must take the form $E_z = \left[A_1 H_0^{(2)}(k_1 r) + B_1 H_0^{(1)}(k_1 r)\right] e^{-jk_z z}$. The core fields given in Table 1 are used to compute the amplitudes of the fields in the first layer, and the points of zeros and peaks are then obtained. Defining a Bessel-tangent function of order m by $\text{Besstan}_m(\cdot) \triangleq Y_m(\cdot)/J_m(\cdot)$, and defining the quantity,

$$U^{(\text{TM})} \triangleq \frac{\dfrac{\varepsilon_1}{k_1} Y_1(k_1 R_{\text{int}}) J_0(k_r R_{\text{int}}) - \dfrac{1}{k_r} Y_0(k_1 R_{\text{int}}) J_1(k_r R_{\text{int}})}{\dfrac{\varepsilon_1}{k_1} J_1(k_1 R_{\text{int}}) J_0(k_r R_{\text{int}}) - \dfrac{1}{k_r} J_0(k_1 R_{\text{int}}) J_1(k_r R_{\text{int}})}\,, \tag{8}$$

the result for the cylindrical TM case is given by

$$\Delta_1^{(\text{TM})} = \begin{cases} \dfrac{1}{k_1}\,\text{arcBesstan}_0\left(U^{(\text{TM})}\right) - R_{\text{int}} & Z_1 > Z_2 \\ \dfrac{1}{k_1}\,\text{arcBesstan}_1\left(U^{(\text{TM})}\right) - R_{\text{int}} & Z_1 < Z_2\,. \end{cases} \tag{9}$$

#4356 - $15.00 US
Received 27 May 2004; revised 1 July 2004; accepted 1 July 2004

Here the smallest value for which $\Delta_1^{(\mathrm{TM})}$ is positive is chosen. For the special case of $v_{\mathrm{ph}} = c$, $U^{(\mathrm{TM})}$ simplifies to read

$$U^{(\mathrm{TM})} = \frac{\frac{\varepsilon_1}{k_1} Y_1(k_1 R_{\mathrm{int}}) - \frac{R_{\mathrm{int}}}{2} Y_0(k_1 R_{\mathrm{int}})}{\frac{\varepsilon_1}{k_1} J_1(k_1 R_{\mathrm{int}}) - \frac{R_{\mathrm{int}}}{2} J_0(k_1 R_{\mathrm{int}})}. \tag{10}$$

For the TE mode, $U^{(\mathrm{TM})}$ is replaced by

$$U^{(\mathrm{TE})} \triangleq \frac{\frac{1}{k_1} Y_1(k_1 R_{\mathrm{int}}) J_0(k_r R_{\mathrm{int}}) - \frac{1}{k_r} Y_0(k_1 R_{\mathrm{int}}) J_1(k_r R_{\mathrm{int}})}{\frac{1}{k_1} J_1(k_1 R_{\mathrm{int}}) J_0(k_r R_{\mathrm{int}}) - \frac{1}{k_r} J_0(k_1 R_{\mathrm{int}}) J_1(k_r R_{\mathrm{int}})} \tag{11}$$

and the condition on the impedances turns into a condition on the admittances, similarly to the planar case. The second curve from the bottom of Fig. 2 corresponds to the cylindrical TM first layer width, and the first curve from the top to the TE case.

3. Effect of matching layer on waveguide characteristics

3.1. Field distribution

With the same given set of two dielectric materials and a given core dimension, the design procedure described above makes it possible to achieve different phase velocities, and correspondingly, different field distributions across the core. As a demonstration of the ability to control the field behavior in the core, the symmetric planar TM mode will next be considered. Figure 3 presents different configurations, where in all cases the core half-width is $D_{\mathrm{int}} = 1\lambda_0$, and the two materials used have refractive indices of 1.6 and 4.6. In all cases the longitudinal electric field across the waveguide E_z is indicated by a solid blue line, and the transverse magnetic field H_y is indicated by a dashed red line. The dielectric layers are depicted in gray, where the higher refractive index layers are indicated by the darker gray.

As a first example, let us consider the case $v_{\mathrm{ph}} = c$ ($k_z = \omega_0/c$), in which the transverse impedance for the first layer, which is given by $Z_1 = k_1/(\omega\varepsilon_0\varepsilon_1)$, takes the form $Z_1 = \eta_0\sqrt{\varepsilon_1 - 1}/\varepsilon_1$. For the materials chosen here, this entails that the higher refractive index material has the lower transverse impedance and vice versa. Placing the material with the lower refractive index adjacent to the hollow core, and setting the matching layer width according to Eq. (5), the field profile of E_z depicted in Fig. 3(a) is uniform across the core. As indicated by Eq. (3) the longitudinal electric field vanishes and the transverse magnetic field peaks at the interface between the first and the second dielectric layers, identically to the case of a metallic wall located at that interface. Maintaining the same field distribution in the core itself, Fig. 3(b) illustrates the case where for $v_{\mathrm{ph}} = c$, the material with the higher refractive index borders the core. Here the second case of Eq. (5) is considered, and the profile obtained is as if a perfect magnetic wall is placed at the interface between the first and the second layers.

As examples of arbitrary field profiles that can be achieved setting the matching layer width according to Eq.(4), Fig. 3(c) and Fig. 3(d), where the transverse wavenumbers were chosen to be $k_x D_{\mathrm{int}} = \pi/3$ and $k_x D_{\mathrm{int}} = 3\pi/4$ respectively, are shown. Finally, as a special case of Eq.(4), the field distributions when all the layers are transverse quarter-wave thick, are shown. Figure 3(e) illustrates the case $k_x D_{\mathrm{int}} = \pi/2$, in which the field in the core behaves as if the core boundary is a metallic wall. Figure 3(f) illustrates the case $k_x D_{\mathrm{int}} = \pi$, which has an identical field to a perfect magnetic wall at the core boundary. It is important to reiterate that common to all cases presented is that at every interface between any two dielectrics, each one of the fields either peaks or vanishes.

#4356 - $15.00 US
Received 27 May 2004; revised 1 July 2004; accepted 1 July 2004

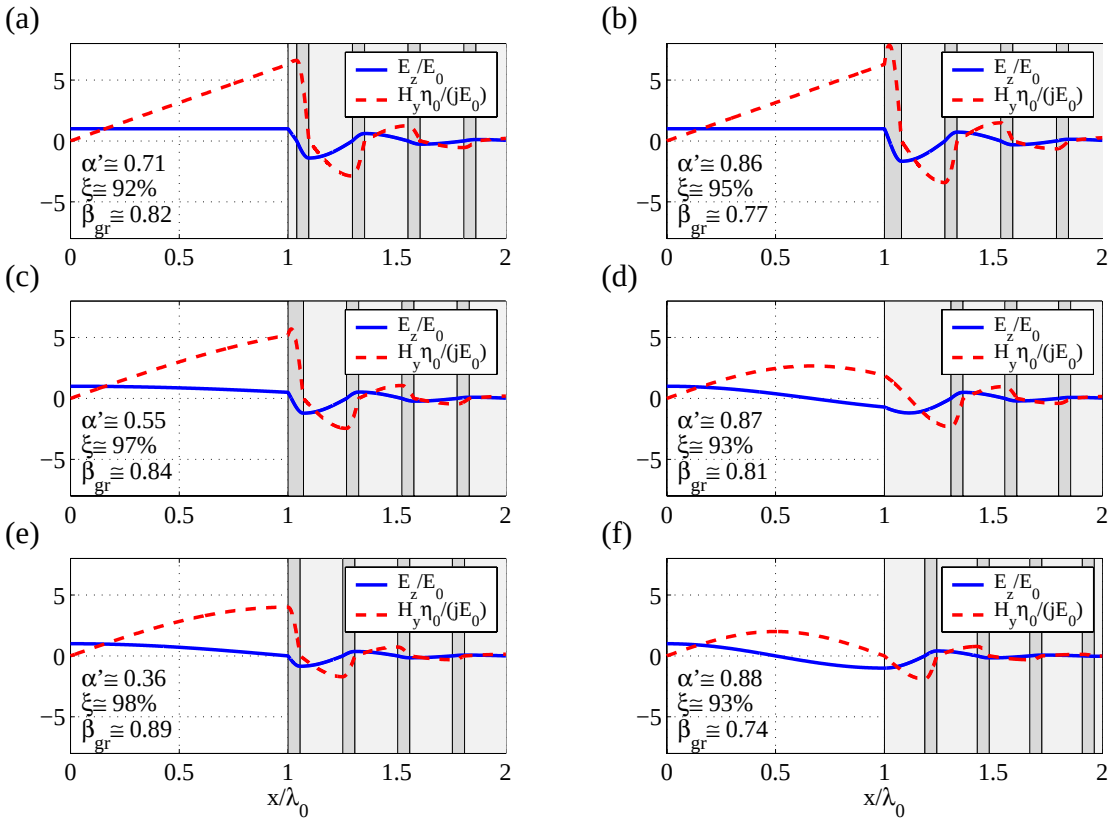

Fig. 3. Planar TM profiles. (a) $k_x D_{\text{int}} = 0$ low refractive index first (b) $k_x D_{\text{int}} = 0$ high refractive index first (c) $k_x D_{\text{int}} = \pi/3$ (d) $k_x D_{\text{int}} = 3\pi/4$ (e) $k_x D_{\text{int}} = \pi/2$ (metallic-like walls) (f) $k_x D_{\text{int}} = \pi$ (magnetic-like walls).

3.2. *Dissipation losses, confined power, and group velocity*

Changing the field distribution inside the core is expected to influence the dissipation losses in the dielectrics. The flowing power P in the waveguide may be written in the form $P(z) = P(0)e^{-2\alpha z}$, where the decay coefficient α is given by

$$\alpha = \frac{2\omega_0 \tan\delta \, W_{\text{E,clad}}(z)}{P(z)}. \tag{12}$$

In the above expression it is assumed for simplicity that both materials have the same loss tangent $\tan\delta$, and $W_{\text{E,clad}}$ represents the electromagnetic energy per unit length (per unit area for the planar case where $\partial/\partial y = 0$) within the dielectric materials. The normalized decay coefficient $\alpha' \triangleq \alpha\lambda_0/\tan\delta$ is indicated on every frame of Fig. 3. Another parameter of interest from the perspective of high power waveguides is the ratio of the power flowing in the core to the total power, denoted by ξ, and is also given for each case of Fig. 3. Although for all cases, ξ is above 90%, α' exhibits more significant variations. It is evident that the best performance is achieved for the metallic-like case (Fig. 3(e)), and the worse is in the magnetic-like case (Fig. 3(f)). The dissipation coefficient in the magnetic-like case is almost 2.5 times greater than that of the metallic-like. In addition to the two parameters discussed above, the normalized group velocity $\beta_{\text{gr}} \triangleq v_{\text{gr}}/c$ is indicated on every frame of Fig. 3. This quantity may be computed

#4356 - $15.00 US
Received 27 May 2004; revised 1 July 2004; accepted 1 July 2004

by the ratio of the total flowing power to the electromagnetic energy per unit length, i.e., the energy velocity, which is known to be equal to the group velocity if the dielectric material is frequency independent [19].

In Table 2 a comparison is made between the TM cases of Fig. 3 and the analogous TE cases[1]. The analogy is in the sense that H_z in the TE case has a similar profile to E_z in the TM case. As expected, the TE(f) profile, which has metallic-like core boundary has the smallest dissipation losses, and the highest percentage of confined power. All the other TE profiles have higher losses and less confined power than all the TM profiles. It should be noted that having over 90% of the power confined in the core for the TM and TE(f) cases is a result of the choice of the refractive indices. The large difference between the materials' indices results in a high ratio between the transverse wave impedances, which are different for the TM and TE cases. It can also be seen that for the TE profiles the group velocity has a greater variance than for the TM profiles.

Table 2. Comparison between the waveguide parameters that correspond to the field distributions of Fig. 3 and the analogous TE cases.

	(a)		(b)		(c)		(d)		(e)		(f)	
	TM	TE	TM	TE	TM	TE	TM	TE	TM	TE	TM	TE
α'	0.71	2.50	0.86	2.54	0.55	2.20	0.87	3.56	0.36	1.73	0.88	0.08
$\xi[\%]$	92.1	74.8	94.8	72.1	96.7	76.5	93.1	88.3	98.0	82.1	92.5	99.7
β_{gr}	0.82	0.65	0.77	0.65	0.84	0.68	0.81	0.48	0.89	0.72	0.74	0.85

3.3. Dispersion curves

So far we have considered only the electromagnetic field behavior at the specific wavelength λ_0, for which the waveguide was designed. As is demonstrated next, adjusting the first layer width, may have a significant effect on the dispersion curve. The dispersion points are determined by searching numerically for the zeros of the dispersion function, which has an analytical expression in the planar case. For the cylindrical case, the transfer matrix method of Ref. [2] is used to determine the reflection coefficient from the outer layers. Taking a relatively large number of layers, the reflection coefficient within the band-gap represents that of an infinite number of layers, i.e., its absolute value is unity for all practical purposes.

First, we examine the symmetric TM mode of both planar and cylindrical Bragg reflection waveguides with $D_{\mathrm{int}} = 0.3\lambda_0$ and $R_{\mathrm{int}} = 0.3\lambda_0$. For the layer adjacent to the core, the material with the *lower* refractive index was chosen. In the left frame of Fig. 4, a band diagram is shown, with the transverse pass-bands of the infinite periodic structure plotted in gray, and the dispersion curves of the symmetric TM mode in the planar case are depicted for two configurations. In the first configuration, plotted in red, all the layers are $\lambda_0/(4\sqrt{\varepsilon-1})$ thick, meaning that the Bragg mirror is designed for $v_{\mathrm{ph}} = c$, but without using a matching layer to match between the mirror and the core field. The result is that the red line does not intersect the point $(\frac{\omega}{\omega_0}, \frac{k_z c}{\omega_0}) = (1,1)$, as is required. Nevertheless, this dispersion curve intersects the light-line at a lower frequency. Operating the waveguide at that frequency is not desirable since the mirror is not optimal, i.e., the transverse exponential decay is weaker than could be achieved. When the first layer is adjusted according to the design procedure described above, the blue curve is obtained. It is seen that changing the first layer thickness shifts the dispersion curve so that

[1]For the TE case (a), $\Delta_1 \sim 10^{-3}\lambda_0$, which is impractical and shown here for comparison purposes only.

#4356 - $15.00 US
Received 27 May 2004; revised 1 July 2004; accepted 1 July 2004

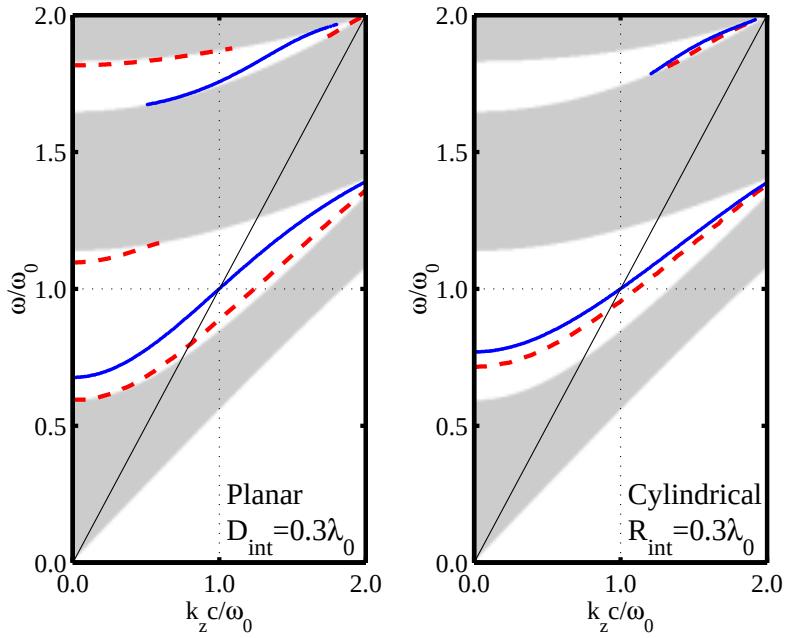

Fig. 4. Symmetric TM mode dispersion diagram for planar waveguide with $D_{\text{int}} = 0.3\lambda_0$ (left) and cylindrical waveguide with $R_{\text{int}} = 0.3\lambda_0$ (right). In both cases the red (dashed) curves are obtained with no design procedure, and the blue (solid) curves correspond to a $v_{\text{ph}} = c$ design procedure.

there is an intersection with the point $(\frac{\omega}{\omega_0}, \frac{k_z c}{\omega_0}) = (1,1)$. A similar picture is obtained for the cylindrical case shown in the right frame of Fig. 4.

In Fig. 5 we repeat the simulations shown in Fig. 4 where the core dimension is now $1.0\lambda_0$ instead of $0.3\lambda_0$. In the left frame, the red curve, indicating the symmetric planar TM mode without a matching layer does not intersect the light-line at the first band-gap. Only by creating a matching layer, an intersection with the light-line at the correct frequency is obtained (blue curve). Hence, the significance of the matching layer is evident.

3.4. Group velocity dispersion

A quantity of interest is the group velocity dispersion. For convenience we choose $\lambda_0 = 1.55\mu m$ as in Refs. [10, 14], and in Fig. 6 the group velocity dispersion is given for the symmetric TM mode that intersects the light-line at this particular wavelngth, as a result of the design procedure. The dotted red curve represents the case $R_{\text{int}} = 0.3\lambda_0$. Adjusting, the internal radius, while rearranging the layers around it so that the condition $v_{\text{ph}} = c$ still holds at λ_0, it is seen that for $R_{\text{int}} = 0.422\lambda_0$ a zero group velocity dispersion point is obtained at $\lambda_0 = 1.55\mu m$. From the perspective of communication applications, the values shown here, being relatively large, may be suitable for dispersion compensation purposes as discussed in Ref. [10], meaning that the zero-dispersion point itself will not be used. On the other hand, considering that high power waveguides, and in particular acceleration modules may be significantly shorter than optical fibers for long distance communication, the zero group-velocity dispersion shown here may be of use. To exemplify this dramatic difference, an estimation of the length of a future optical acceleration module is of the order of a few millimeters, which is more than 6 orders of magnitude shorter than an optical fiber for communication purposes. Consequently, an adjustment of

#4356 - $15.00 US
Received 27 May 2004; revised 1 July 2004; accepted 1 July 2004

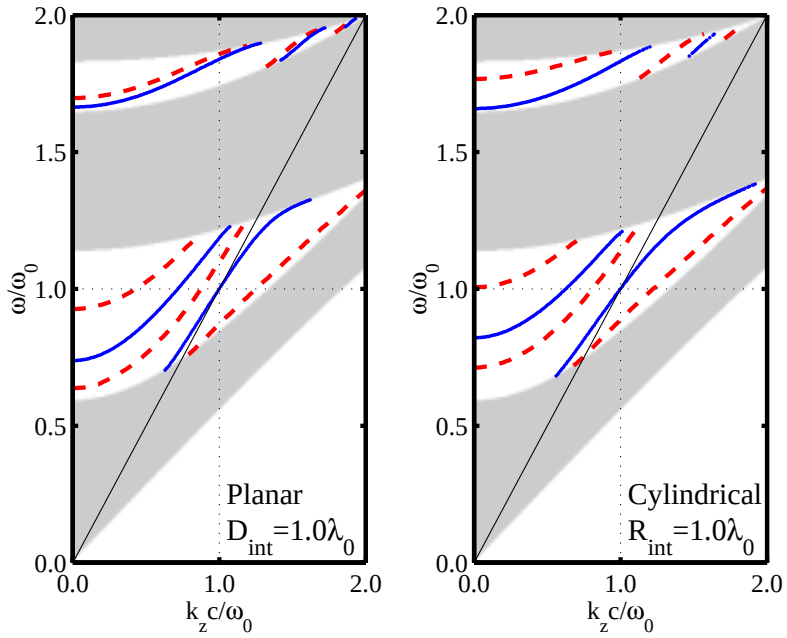

Fig. 5. Symmetric TM mode dispersion diagram for planar waveguide with $D_{\text{int}} = 1.0\lambda_0$ (left) and cylindrical waveguide with $R_{\text{int}} = 1.0\lambda_0$ (right). In both cases the red (dashed) curves are obtained with no design procedure, and the blue (solid) curves correspond to a $v_{\text{ph}} = c$ design procedure.

the core dimension to achieve a zero group velocity dispersion may be valuable.

4. Planar odd modes

The core field distributions given in Table 1 for the planar case are *even* modes that have the property that the longitudinal Poynting vector S_z vanishes on axis. In applications such as high power waveguides or dielectric particle manipulation by light [16], this could be a major drawback. A way to overcome this problem is to use an odd mode (for example TM) of the form

$$\begin{aligned} E_z &= E_0 \sin(k_x x) e^{-jk_z z}, \\ E_x &= -j\frac{k_z}{k_x} E_0 \cos(k_x x) e^{-jk_z}, \\ H_y &= -j\frac{\omega_0 \varepsilon_0}{k_x} E_0 \cos(k_x x) e^{-jk_z z}. \end{aligned} \tag{13}$$

By the same method discussed above it is possible to confine the odd mode with a matching layer with a width that has a similar expression to the even mode case

$$\Delta_1^{(\text{TM})} = \begin{cases} \dfrac{1}{k_1} \arctan\left[-\dfrac{\varepsilon_1 k_x}{k_1} \tan(k_x D_{\text{int}})\right] & Z_1 > Z_2 \\ \dfrac{1}{k_1} \arctan\left[\dfrac{k_1}{\varepsilon_1 k_x} \cot(k_x D_{\text{int}})\right] & Z_1 < Z_2 . \end{cases} \tag{14}$$

It is now possible to create a desired power profile within the core, with non-zero value on axis. Two possibilities for this are presented in Fig. 7, in which the longitudinal Poynting vector nor-

#4356 - $15.00 US
Received 27 May 2004; revised 1 July 2004; accepted 1 July 2004

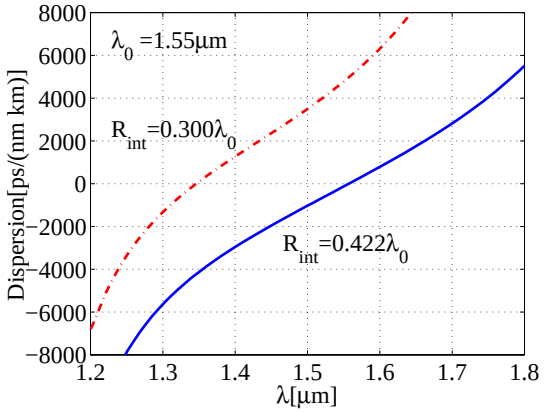

Fig. 6. Group velocity dispersion for the $v_{\mathrm{ph}} = c$ cylindrical waveguide.

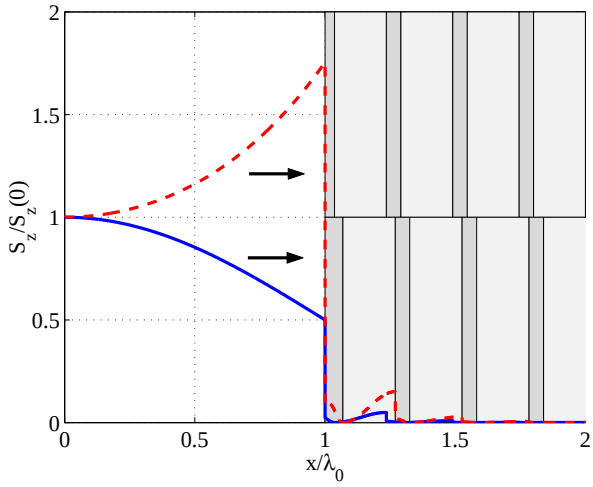

Fig. 7. Planar odd TM power profiles: $k_x D_{\mathrm{int}} = \pi/4$ (solid blue) and $k_x D_{\mathrm{int}} = j\pi/4$ (dashed red).

malized to its value on axis is depicted for $k_x D_{\mathrm{int}} = \pi/4$ (solid blue) and $k_x D_{\mathrm{int}} = j\pi/4$ (dashed red). In the first case the axis value is maximal, and in the second case the cosine function (in E_x and H_y) turns into a hyperbolic cosine, and therefore the axis value is the minimum. In each one of the cases the locations of the layers are indicated, showing that the different width of the matching layer enables the mode to be supported. In the application of dielectric particle levitation, the transverse distribution of the "propelling" power may be crucial for the transverse stability of the levitated body.

5. Hollow-region-TEM in planar and coaxial Bragg waveguides

In the previous section, we have shown for the planar waveguide that it is possible to create a core power distribution with either monotonically increasing or monotonically decreasing profile, and non-zero on axis. A special case is when the power profile is completely flat within the core, meaning that inside the core the field is pure TEM ($k_x = 0$, $k_z = \omega_0/c$), having both

#4356 - $15.00 US
Received 27 May 2004; revised 1 July 2004; accepted 1 July 2004

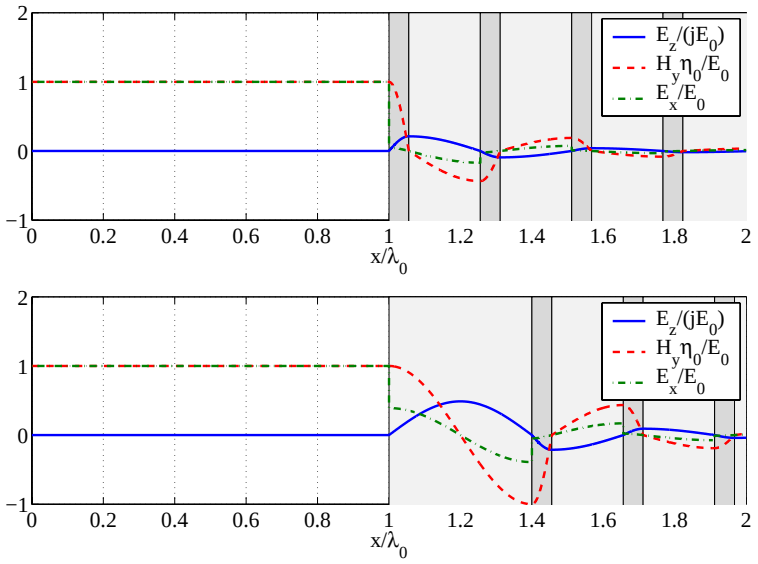

Fig. 8. Planar TEM-TM profiles: higher refractive index first (top) and lower refractive index first (bottom).

$E_z \equiv 0$ and $H_z \equiv 0$. In the dielectric layers the field must be either TM or TE, and the waveguide may be matched to either. By computing the amplitudes in the layer adjacent to the core, we find for the TEM-TM that the first layer should either be transverse quarter-wavelength thick for $Z_1 < Z_2$ (higher refractive index first for the materials chosen here), meaning that actually no matching to the Bragg mirror is needed, or transverse half-wavelength thick for $Z_1 > Z_2$. This conclusion is independent of the internal half-width D_{int}. All three fields, E_z, E_x, and H_y are plotted in Fig. 8 for both cases. A TEM-TE mode would have H_z, H_x, and E_y, and no matching to the mirror is needed if the higher TE admittance material is first, and a transverse half-wavelength is required if lower admittance is first.

Creating a similar TEM mode in the cylindrical structure is possible only by adding a dielectric material around the axis, turning the waveguide into a dielectric coaxial cable, a device which was analyzed before [11, 12, 13]. The approach presented in this paper of tailoring the waveguide discontinuities around a specified field distribution is applicable here as well. As an example, let us consider a TEM-TM mode, entailing $k_z = \omega_0/c$. The configuration considered is of a dielectric rod with relative permittivity ε_r of radius R_{int}, a hollow region in $R_{\text{int}} < r < R_{\text{ext}}$, and dielectric layers for $r > R_{\text{ext}}$. The electromagnetic field within the dielectric rod are of the form

$$\begin{aligned} E_z &= E_0 J_0(k_r r) e^{-jk_z z}, \\ E_r &= \frac{j}{\eta_0} \frac{\varepsilon_r}{\sqrt{\varepsilon_r - 1}} E_0 J_1(k_r r) e^{-jk_z z}, \\ H_\phi &= \frac{j}{\sqrt{\varepsilon_r - 1}} E_0 J_1(k_r r) e^{-jk_z z}. \end{aligned} \tag{15}$$

At the hollow region we require that the TEM mode will exist, i.e., the only field components

#4356 - $15.00 US
Received 27 May 2004; revised 1 July 2004; accepted 1 July 2004

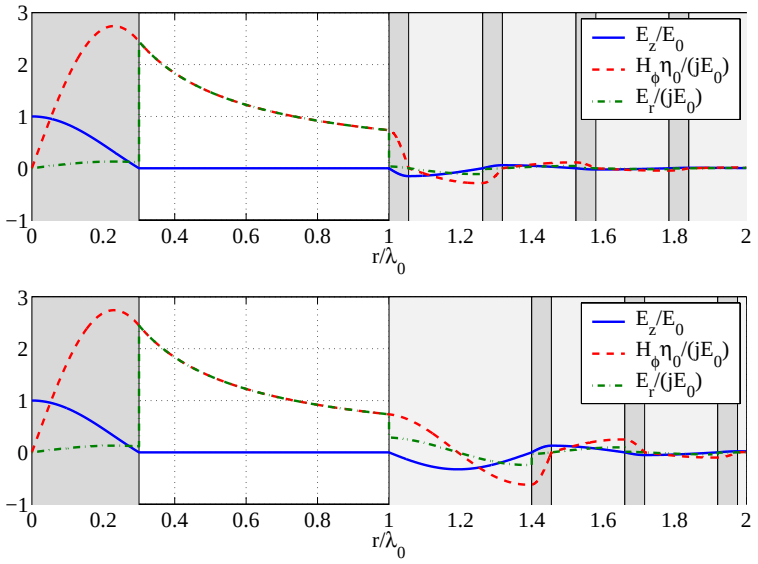

Fig. 9. Coaxial TEM-TM profiles: the higher refractive index is first at the hollow region outer boundary (top) and the lower refractive index first (bottom).

are

$$E_r = \frac{C}{\eta_0}\frac{1}{r}e^{-jk_z z}, \qquad H_\phi = \frac{C}{r}e^{-jk_z z}. \tag{16}$$

Since $E_z = 0$ at the hollow part, the internal dielectric rod must be designed so that E_z vanishes at the boundary, entailing $k_r R_{\text{int}} = p_1$, where p_1 is the first zero of the Bessel function $J_0(\cdot)$. Imposing the continuity of H_ϕ, we get for the coefficient $C = j\frac{\varepsilon_r}{\sqrt{\varepsilon_r - 1}}J_1(p_1)R_{\text{int}}E_0$. The dielectric internal rod may be conceived as a matching layer between the field on axis to the TEM mode in the hollow region. It is now possible to proceed as before to the next discontinuity located at $r = R_{\text{ext}}$, and impose the boundary conditions there with the TM mode at the first dielectric layer. The next interfaces will be placed where E_z either peaks or vanishes, as before. In Fig. 9 the three field components E_z, E_r, and H_ϕ are plotted. The dielectric rod was taken to have $\varepsilon_r = 4.6^2$, as one of the dielectrics composing the Bragg mirror. Similarly to the planar case, at the top frame, when the material with the lower impedance is first, virtually no matching is required and the first layer is almost transverse quarter-wavelength thick. If the material with the higher impedance is placed first, the first layer is required to be transverse half-wavelength thick. Matching a TEM-TE mode is also possible, similarly to the way described in the planar case, where the three field components would be H_z, H_r and E_ϕ, with zero H_z in the hollow region. For the TEM-TM mode, as shown in Fig. 9, the longitudinal electric field E_z vanishes at the boundaries of the hollow region similarly to the metallic coaxial cable. In the TEM-TE case the longitudinal magnetic field would vanish, similarly to a coaxial waveguide with perfect magnetic walls. Obviously, the same design procedure can be carried out if the internal rod has more than one dielectric layer.

#4356 - $15.00 US
Received 27 May 2004; revised 1 July 2004; accepted 1 July 2004

6. Conclusion

A general design procedure for supporting a specified symmetric mode, TM, TE or TEM, in an either planar or cylindrical Bragg reflection waveguide was given. The locations of the interfaces between the dielectric layers are placed so that the boundary conditions on the electromagnetic field are fulfilled. For that to occur, a matching layer is required between the electromagnetic field within the core, and the Bragg mirror designed for that specific transverse wavelength. The matching layer provides an important tool for controlling the phase velocity, the field distribution, and the power distribution within the core.

Analytical expressions for the first layer width in several configurations were given. As a special case, the configuration where the layers are all transverse quarter-wavelength thick (no matching layer), was obtained. It was shown that the Bragg reflection waveguide with a matching layer behaves at the operation wavelength as a metallic dielectric loaded or perfect magnetic dielectric loaded waveguide, since at the interface between the first and the second layers the fields either peak or vanish. The case where all layers are transverse quarter-wavelength thick results in a behavior of either a metallic wall or a perfect magnetic wall at the core boundary.

The effect of adjusting the first layer width on waveguide characteristics was discussed in terms of the dissipation losses, confined power and the group velocity. Moreover, the matching layer may change significantly the dispersion curves, to intersect with the specified point.

For planar Bragg reflection waveguides, it was shown that odd modes may be supported to give power density profiles with non-zero power on axis and specified properties, and specifically the power density gradient may be controlled. This may be useful in high power waveguides, or for dielectric particle manipulation. Furthermore, planar Bragg reflection waveguides were shown to support TEM-TM, or TEM-TE modes, where the power profile inside the core is flat. Similarly, a systematic design procedure for supporting a TEM-TM or TEM-TE mode in a coaxial fiber was given.

It is possible to further generalize the concept of the matching layer to matching with more than one layer or matching to a mirror which is not optimal for the given mode. In this last case, the eigen-vectors of the periodic structure will entail that the fields do not peak or vanish at the interface, but there is some phase between the outgoing and incoming transverse waves.

Acknowledgments

This study was supported by the Israeli Science Foundation.

#4356 - $15.00 US Received 27 May 2004; revised 1 July 2004; accepted 1 July 2004